

# Complexity in transition metal oxides

Gonzalo Alvarez<sup>a</sup>, Adriana Moreo<sup>b</sup> and Elbio Dagotto<sup>b</sup>

<sup>a</sup> Computer Science & Mathematics Division, Oak Ridge National Laboratory, Oak Ridge, Tennessee 37831, USA

<sup>b</sup> Condensed Matter Sciences Division, Oak Ridge National Laboratory, Oak Ridge, Tennessee and Department of Physics and Astronomy, The University of Tennessee, Knoxville, Tennessee 37996, USA

## ABSTRACT

The competition of antiferromagnetic and  $d$ -wave superconductivity order parameters in cuprates is studied within a phenomenological model. An unbiased numerical analysis is carried out. The results suggest that the transition from the antiferromagnetic to the superconducting region is not universal. When disorder is present, a glassy state forms leading to the possibility of “colossal” effects in some cuprates, analog of those in other transition metal oxides, in particular manganites. Non-superconducting Cu-oxides could rapidly become superconducting by the influence of weak perturbations. Consequences of this mechanism for thin-film and angle-resolved photoemission experiments are discussed. In addition, a recent study of the strong-coupling region in  $d$ -wave superconductors with a numerically exact technique is briefly reviewed.

**Keywords:** superconductors,  $d$ -wave, clustered states, pseudo-gap

## 1. INTRODUCTION

Clarifying the physics of high-temperature superconductors (HTSs) is still one of the most important challenges in condensed-matter physics. There is overwhelming experimental evidence for several unconventional regimes in HTSs, including a pseudogap region at temperatures above the superconducting (SC) phase, and a largely unexplored glassy state separating the parent antiferromagnet (AF) from the SC phase at low hole-doping  $x$ . It is argued that different inhomogeneous states could be stabilized in different Cu-oxides, depending on coupling and quenched disorder strengths. In fact, neutron scattering studies have revealed “stripes” of charge in Nd-LSCO,<sup>1,2</sup> but scanning tunneling microscopy (STM) experiments<sup>3,4</sup> indicate “patches” in Bi2212, consistent with our analysis. There is no unique way to transition from AF to SC. Two models are used, one with itinerant fermions (Section 2) and the other without (Section 3), and the conclusions are similar in both.

In addition, recent investigations unveiled another remarkable property of HTSs that defies conventional wisdom: the existence of *giant proximity effects* (GPE) in some cuprates,<sup>5–7</sup> where a supercurrent in Josephson junctions was found to run through non-SC Cu-oxide-based thick barriers. This contradicts the expected exponential suppression of supercurrents with barrier thickness beyond the short coherence length of Cu-oxides. We will review in Section 4 a recent explanation<sup>8</sup> based on a description of the glassy state as containing SC *puddles*. This nanoscale inhomogeneous state leads to *colossal effects in cuprates*, in analogy with manganites.<sup>9–11</sup>

In Section 5 the dependence of  $T_C$  with the number of Copper oxide layers is reviewed. This is very relevant in view of the fact that due to the Mermin-Wagner theorem for Hubbard and similar models,<sup>12,13</sup> finite-temperature phase transitions are not possible when considering short range interactions in the Hamiltonian on a two-dimensional system. Therefore, the influence of other layers is thought to stabilize the transition. In finite systems we have found that  $T_C$  indeed increases rapidly with an increasing number of layers.

The form of the spectral functions in the presence of competing AF and SC states is presented in Section 6 following Ref. 14. One of the main results of this section is that the spectral function of the system without quenched disorder cannot reproduce the angle-resolved photoemission spectroscopy (ARPES) data but that quenched disorder is indeed crucial.

Another important and related issue is the study of  $d$ -wave superconductors’ strong coupling regime. This regime is sometimes attributed to be responsible for the properties observed in the pseudogap region mentioned

previously. If this is the case, then conventional mean-field (MF) methods should not work in describing the cuprates, since they cannot distinguish between the temperatures for the formation of long and short range orders. Therefore, we review in Section 7 recently proposed<sup>15</sup> Monte Carlo techniques to address this problem within a numerical exact approach and the results obtained with them.

Studies of the  $t$ - $J$  model have revealed SC and striped states<sup>16,17</sup> evolving from the undoped limit. Then, it is reasonable to assume that AF, SC, and striped states are dominant in cuprates, and their competition regulates the HTS phenomenology. However, further computational progress using basic models is limited by cluster sizes that cannot handle the nanoscale structure unveiled by STM experiments. Considering these restrictions, here a *phenomenological* approach will be pursued to understand how these phases compete, incorporating the quenched disorder inevitably introduced by chemical doping. This effort unveils novel effects of experimental relevance, not captured with first-principles studies. Hopefully, the results and methods reviewed here will jump start a more detailed computational analysis of phenomenological models in the high- $T_c$  arena, since most basic first-principles approaches, including Hubbard and  $t - J$  investigations, have basically reached their limits, particularly regarding lattice sizes that can be studied.

## 2. MODEL I: ITINERANT FERMIONS

The analysis starts with a phenomenological model of itinerant electrons (simulating carriers) on a square lattice, locally coupled to classical order parameters:

$$\begin{aligned}
H_F = & -t \sum_{\langle ij \rangle, \sigma} (c_{i\sigma}^\dagger c_{j\sigma} + H.c.) + 2 \sum_{\mathbf{i}} J_i S_i^z s_i^z - \sum_{\mathbf{i}\sigma} \mu_i n_{i\sigma} \\
& + \frac{1}{D} \sum_{\mathbf{i}, \alpha} \frac{1}{V_i} |\Delta_{i\alpha}|^2 - \sum_{\mathbf{i}, \alpha} (\Delta_{i\alpha} c_{i\uparrow} c_{i+\alpha\downarrow} + H.c.), \tag{1}
\end{aligned}$$

where  $c_{i\sigma}$  are fermionic operators,  $s_i^z = (n_{i\uparrow} - n_{i\downarrow})/2$ ,  $n_{i\sigma}$  is the number operator,  $D$  is the lattice dimension, and  $\Delta_{i\alpha} = |\Delta_{i\alpha}| e^{i\phi_i^\alpha}$  are complex numbers for the SC order parameter defined at the links  $(\mathbf{i}, \mathbf{i}+\alpha)$  ( $\alpha =$  unit vector along the  $x$  or  $y$  directions). At  $J_i=0$ ,  $d$ -wave SC is favored close to half-filling since the pairing term involves nearest-neighbor sites, as in any standard mean-field approximation to SC. The spin degrees of freedom (d.o.f.) are assumed to be Ising spins (denoted by  $S_i^z$ ). Studies with  $O(3)$  d.o.f. were found to lead to qualitatively similar conclusions, but they are more CPU time consuming. The parameters of relevance are  $J_i$ ,  $\mu_i$ , and  $V_i$  ( $t$  is the energy unit), that carry a site dependence to easily include quenched disorder which is inevitable in chemically doped compounds as the cuprates. For a fixed configuration,  $\{\Delta_{i\alpha}\}$  and  $\{S_i^z\}$ , the one-particle sector is Bogoliubov diagonalized using the transformation:

$$\begin{aligned}
c_{i\uparrow} &= \sum_{n=1}^{n=N} \{a_n(\mathbf{i})\gamma_{n\uparrow} - b_{n+N}^*(\mathbf{i})\gamma_{n\downarrow}^\dagger\}, \\
c_{i\downarrow} &= \sum_{n=1}^{n=N} \{b_n(\mathbf{i})\gamma_{n\downarrow} + a_{n+N}^*(\mathbf{i})\gamma_{n\uparrow}^\dagger\}. \tag{2}
\end{aligned}$$

$a_n(\mathbf{i})$  and  $b_n(\mathbf{i})$  in (2) are complex numbers and are chosen so that a Hamiltonian that is diagonal in  $\gamma_{n\sigma}$  emerges. In the limit  $T \rightarrow 0$ , the Bogoliubov-de Gennes equations are recovered minimizing the energy.<sup>18-20</sup> Then, a standard Monte Carlo (MC) simulation similar to those for Kondo-lattice models is carried out (details in Ref. 9). One of the goals is to estimate  $T_c$ , as well as  $T_c^*$ , roughly defined as the temperature at which strong short-distance SC correlations develop.

### 2.1. Phase Diagram in the Clean Limit

Without quenched disorder,  $V_i$ ,  $J_i$  and  $\mu_i$  in Eq. (1) are site independent. The standard MC analysis carried out in these investigations reveals that in the clean limit the low temperature ( $T$ ) phase diagram, Fig.1(a), has a

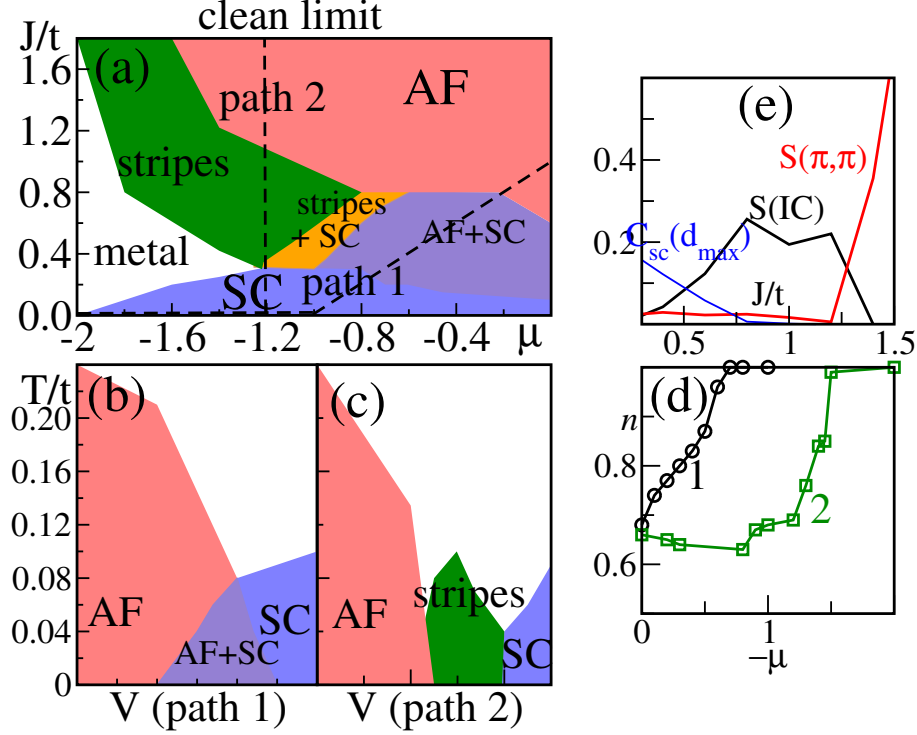


**Figure 1.** (a) MC phase diagram for Eq. (1) without disorder at low temperatures. Instead of presenting a three dimensional phase diagram we have chosen to present a two dimensional cut along  $V=1-J/2$  for simplicity. Five regions are observed: AF,  $d$ -SC, stripes, coexisting SC+AF, coexisting stripes+SC, and metallic. (b) MC phase diagram including temperature along “Path 1”. (c) MC phase diagram along “Path 2”. Lattice sizes in all cases are  $8\times 8$  and  $12\times 12$ . (d)  $n$  vs.  $\mu$  along Paths 1 and 2. Transitions along Path 1 appear continuous, whereas along Path 2 there are indications of first-order transitions. (e) Spin structure factor  $S(\mathbf{q})$  at  $(\pi, \pi)$  and for incommensurate (IC) momenta. (Adapted from Ref. 8)

robust AF phase for electronic densities  $n\sim 1$  and a  $d$ -wave SC phase for  $n<1$ . The  $d$ -wave correlation function, defined as

$$C_{sc}^{\alpha\beta}(\mathbf{m}) = \sum_{\mathbf{i}} \left\langle |\Delta_{\mathbf{i}}| |\Delta_{\mathbf{i}+\mathbf{m}}| \cos(\phi_{\mathbf{i}}^{\alpha} - \phi_{\mathbf{i}+\mathbf{m}}^{\beta}) \right\rangle, \quad (3)$$

was used to estimate  $T_c$  as the temperature at which  $d$ -wave correlations at the largest distances for the lattices considered here are 5% of their maximum value at  $|\mathbf{m}|=0$ . The 5% criterion is arbitrary but other criteria lead to identical qualitative trends, slightly shifting the phase diagrams.  $T^*$  is deduced similarly, but using the shortest non-zero distance correlation function ( $|\mathbf{m}|=1$ ). The Néel temperature,  $T_N$ , associated with the classical spins was defined by the drastic reduction ( $\leq 5\%$  of  $|\mathbf{m}|=0$  value) of the long-distance spin order using  $C_S(\mathbf{m}) = \sum_{\mathbf{i}} \langle S_{\mathbf{i}}^z S_{\mathbf{i}+\mathbf{m}}^z \rangle$ , while  $T_N^*$  relates to short-range spin order. The results presented in Fig. 1(a) are not surprising since these states are favored explicitly in Eq. (1) by the second and fifth terms, respectively. However, the phase diagram presents several nontrivial interesting regions: (i) Along “Path 1” in Fig. 1(a), the AF-SC transition occurs through *local coexistence*, with tetracritical behavior (Fig. 1(b)).<sup>21</sup> (ii) Along “Path 2” the AF-SC interpolating regime has alternating doped and undoped *stripes* (stripes in MC data are deduced from spin and charge structure factors, and low- $T$  MC snapshots), and a complex phase diagram, Fig. 1(c). These stripes evolve continuously from the  $V=0$  limit that was studied before by Moreo et al., and as a consequence we refer the readers to Ref. 22 for further details on how stripes were identified. It remains to be investigated if these stripes, involving SC and AF quasi-1D lines, have the are originated by the same mechanisms as those widely discussed before in the high- $T_c$  literature.<sup>17, 23–27</sup> At  $V \neq 0$ , the doped regions of the stripes have nonzero SC amplitude at the mean-field level.<sup>28</sup> In view of the dramatically different behavior along Paths 1 and 2, we conclude that

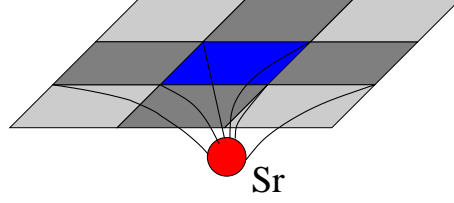


**Figure 2.** Schematic representation of Sr doping. A chemical dopant (Sr) will not only disorder the nearest sites (blue color) in the  $\text{CuO}_2$ -plane, but also neighboring ones, motivating the introduction of “plaquette”-like disorder configurations.

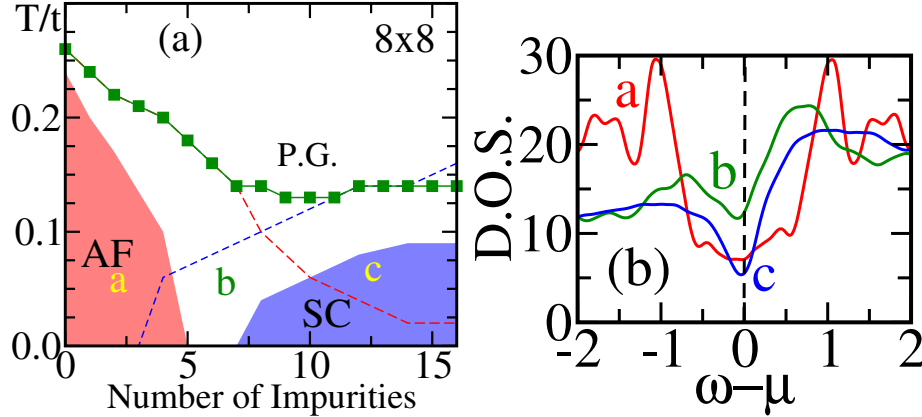


**Figure 3.** (a) MC phase diagram for model Eq. (1) including quenched disorder (lattices studies are  $8 \times 8$  (results shown) and  $12 \times 12$ ). Shown are  $T_c$  and  $T_N$  vs. number of impurities (equal to number of holes). The SC and AF regions with short-range order (dashed lines), and  $T^*$  as obtained from the PG (dot-dashed line) are also indicated. (b) DOS at points  $a$ ,  $b$ , and  $c$  of (a), with a PG. (From Ref. 8)

in our model *there is no unique  $AF \rightarrow SC$  path*. This is in agreement with experiments since  $\text{La}_{2-x}\text{Sr}_x\text{CuO}_4$  (LSCO) and others have stripes,<sup>1,2,29</sup> while  $\text{Ca}_{2-x}\text{Na}_x\text{CuO}_2\text{Cl}_2$  has a more complex inhomogeneous pattern.<sup>4</sup> Both, however, become SC with increasing  $x$ . This suggests that *the underdoped region of Cu-oxides may not be universal*.

## 2.2. Phase Diagram with Quenched Disorder

Our results become even more interesting upon introducing quenched disorder. Disorder may have several forms, but here we mimic Sr-doping in single-layers.  $\text{Sr}^{2+}$  replaces  $\text{La}^{3+}$ , above the center of a Cu-plaquette in the Cu-oxide square lattice. Then, as hole carriers are added, a hole-attractive plaquette-centered potential should also be incorporated as sketched in Fig. 2. Near the center of this potential,  $n$  should be sufficiently reduced from 1 that, phenomenologically, tendencies to SC should be expected. To interpolate between the SC central plaquette and the AF background, a plaquette ‘halo’ with no dominant tendency was introduced. Parameters are chosen such that the blue (black) region favors superconductivity,  $(J, V, \mu) = (0.1, 1.0, -1.0)$ , with a surrounding white region where  $(J, V, \mu) = (0.1, 0.1, -0.5)$  with no order prevailing. The impurity is embedded in a background that favors the AF state,  $(J, V, \mu) = (1.0, 0.1, 0.0)$ . However, the overall conclusions found here are simple, and independent of the disorder details.

The phase diagram obtained with the Monte Carlo simulation is shown in Fig. 3(a). The similarity with the widely accepted phase diagram of the cuprates is clear. The disorder has opened a hole-density “window” where none of the two competing orders dominates. Inspecting “by eye” the dominant MC configurations (snapshots) at low- $T$  in this intermediate regime reveals a patchy system with slowly evolving islands of SC or AF, and random orientations of the local order parameters, leading to an overall disordered “clustered” state. In Fig. 3(a), a new temperature scale  $T^*$  at which the fermionic density-of-states (DOS) develops a *pseudogap* (PG) (Fig. 3(b)) was also unveiled. The AF and  $d$ -SC regions both have a gap (smeared by  $T$  and disorder, but nevertheless with

recognizable features). But even the “disorder” regime (case b in Fig. 3(b)) has a PG. MC snapshots explains this behavior: in the disordered state there are small SC or AF regions, as explained above. Locally each has a smeared-gap DOS, either AF or SC. Not surprisingly, the mixture presents a PG. The behavior of  $T^*$  vs.  $x$  is remarkably similar to that found experimentally. *The cuprates’ PG may arise from an overall-disordered clustered state with local AF or SC tendencies*, without the need to invoke other exotic states. This PG is correlated with robust short-range correlations (dashed lines in Fig.3(a), see caption for details.).

### 3. MODEL II: LANDAU GINZBURG

The results reported thus far, based on Eq. (1), have already revealed interesting information, namely the possible paths from AF to SC, and a proposed explanation of the glassy state as arising from the inevitable quenched disorder in the samples. However, the inhomogeneous nature of the clustered region suggests that percolative phenomena may be at work, and larger clusters are needed. To handle this issue, another model containing *only* classical d.o.f. is proposed, with low-powers interactions typical of Landau-Ginzburg (LG) approaches:

$$\begin{aligned}
H &= r_1 \sum_{\mathbf{i}} |\Delta_{\mathbf{i}}|^2 + \frac{u_1}{2} \sum_{\mathbf{i}} |\Delta_{\mathbf{i}}|^4 + \sum_{\mathbf{i}, \alpha} \rho_2(\mathbf{i}, \alpha) \mathbf{S}_{\mathbf{i}} \cdot \mathbf{S}_{\mathbf{i}+\alpha} \\
&- \sum_{\mathbf{i}, \alpha} \rho_1(\mathbf{i}, \alpha) |\Delta_{\mathbf{i}}| |\Delta_{\mathbf{i}+\alpha}| \cos(\Psi_{\mathbf{i}} - \Psi_{\mathbf{i}+\alpha}) + r_2 \sum_{\mathbf{i}} |\mathbf{S}_{\mathbf{i}}|^2 \\
&+ \frac{u_2}{2} \sum_{\mathbf{i}} |\mathbf{S}_{\mathbf{i}}|^4 + u_{12} \sum_{\mathbf{i}} |\Delta_{\mathbf{i}}|^2 |\mathbf{S}_{\mathbf{i}}|^2.
\end{aligned} \tag{4}$$

The fields  $\Delta_{\mathbf{i}} = |\Delta_{\mathbf{i}}| e^{i\Psi_{\mathbf{i}}}$  are complex numbers representing the SC order parameter. The classical spin at site  $\mathbf{i}$  is  $\mathbf{S}_{\mathbf{i}} = |\mathbf{S}_{\mathbf{i}}| (\sin(\theta_{\mathbf{i}}) \cos(\phi_{\mathbf{i}}), \sin(\theta_{\mathbf{i}}) \sin(\phi_{\mathbf{i}}), \cos(\theta_{\mathbf{i}}))$ .  $\rho_1(\mathbf{i}, \alpha) = 1 - \rho_2(\mathbf{i}, \alpha)$  is used as the analog of  $V = 1 - J/2$  of the previous model to reduce the multiparameter character of the investigation, allowing an AF-SC interpolation changing just one parameter.  $\alpha$  denotes the two directions  $\hat{x}$  and  $\hat{y}$  in 2d, and also  $\hat{z}$  for multilayers.  $\rho_2(\mathbf{i}, \alpha)$  was chosen to be isotropic, i.e.,  $\alpha$ -independent.

#### 3.1. Basic Properties

Clearly, the lowest-energy state for  $\rho_2 = 0$  is a homogeneous SC state (if  $\rho_1(\mathbf{i}, \alpha) = \rho_1^0 > 0$ ). When  $\rho_1 = 0$  the lowest-energy state is AF (if  $\rho_2(\mathbf{i}, \alpha) = \rho_2^0 > 0$ ). In the clean limit, this model was already studied in the SO(5) context, where the reader is referred for further details. Our approach without disorder has similarities with SO(5) ideas<sup>21</sup> where the AF/SC competition as the cause of the high- $T_c$  phase diagram was extensively discussed although nowhere in our investigations we need to invoke a higher symmetry group. The relevance of tetracriticality in  $\text{La}_2\text{CuO}_{4+\delta}$  has also been remarked by E. Demler *et al.*<sup>30</sup> and Y. Sidis.<sup>31</sup> In the present work, disorder is introduced by adding a randomly selected bimodal contribution, i.e.  $\rho_2(\mathbf{i}, \alpha) = \rho_2^0 \pm W$ , where  $W$  is the disorder strength ( $W = 0$  is the clean limit). It is expected that other forms of disorder will lead to similar results.

#### 3.2. Phase Diagram

Monte Carlo results for Eq. (4) are in Fig. 4a, for “weak” coupling  $u_{12} = 0.7$ , which leads to tetracritical behavior. Both at  $W = 0$  and  $W \neq 0$ , the qualitative similarity with fermionic model results (Figs.1(b) and 3(b)) is clear. Coexisting SC and AF clusters appear in MC snapshots (not shown). Then, both models share a similar phenomenology, and Eq. (4) can be studied on larger lattices. The only important difference between the two models is that Eq. (4) cannot lead to doped-undoped stripes, but the more general case Eq. (1) does. Fig. 4(b) illustrates how the phase diagram, Fig. 4(a), was obtained. For completeness, note that increasing the coupling  $u_{12}$  a first-order SC-AF transition can be obtained. However, the addition of disorder leads to a very similar phase diagram as in the case of  $u_{12} = 0.7$ . This is shown in Fig. 4c and is the equivalent of Fig. 4a in the regime of “strong” coupling.

Some of the experimental predictions related with our SC-AF clustered state are simple (the most elaborated ones are in the next section). In most ways a very underdoped cuprate can be tested, there should be two components in the data. For instance, a typical photoemission spectra in our framework should have two

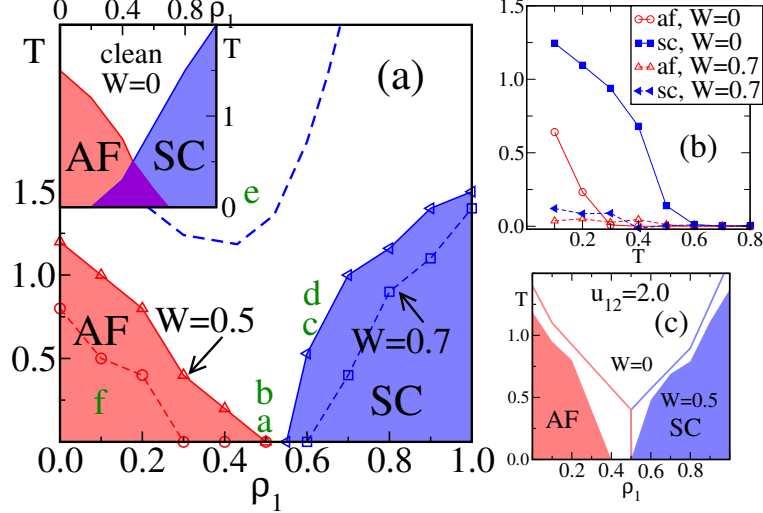


**Figure 4.** (a) MC phase diagram (for Eq. (4)) at  $u_{12}=0.7$ . Parameters are  $r_1=-1$ ,  $r_2=-0.85$ , and  $u_1=u_2=1$  but the conclusions are not dependent on coupling fine-tuning. Spin  $C_{\text{spin}}(\mathbf{m})=\frac{1}{N}\sum_i\langle\mathbf{S}_i\cdot\mathbf{S}_{i+\mathbf{m}}\rangle$  and SC correlations  $C_{\text{SC}}(\mathbf{m})=\frac{1}{N}\sum_i|\Delta_i||\Delta_{i+\mathbf{m}}|\cos(\Psi_i-\Psi_{i+\mathbf{m}})$  were measured. The behavior of these functions at the largest (shortest) distance determine  $T_c$  and  $T_N$  ( $T^*$ ) (same criteria as for Eq. (1)). With disorder, the phase diagram (shown) has an intermediate “clustered” state with short-range order.  $T^*$  is also indicated (dashed line). Note the similarity with Fig. 3(b). *Inset:* results at  $W=0$  showing tetracriticality (magenta (dark) indicates SC-AF coexistence). (b) AF and SC correlations at maximum distance for the model Eq. (4) without and with disorder ( $W=0.0$  and  $0.7$ , respectively).  $\rho_1=0.5$  and  $u_{12}=0.7$  were used, using a  $24\times 24$  lattice. Typically, for the LG model 25,000 sweeps were used for thermalization and measurements. (c) MC phase diagram of model Eq. (4) at  $u_{12}=2.0$ . The clean case ( $W=0$ , solid lines) is bicritical-like, but with disorder  $W=0.5$  a clustered region between SC and AF opens as well. (From Ref. 8)

clearly distinct coexisting signals. This result, which will be discussed in more detail in a future publication, is compatible with photoemission experiments for  $x=0.03$  LSCO, that reveal spectral weight in the node direction of the  $d$ -wave superconductor even in the insulating glassy regime.<sup>32</sup> Nodal  $d$ -wave SC particles surviving to low  $x$  was observed in Ref. 33.

#### 4. GIANT PROXIMITY EFFECT IN CUPRATES

Another important result of these investigations is that the models studied here can present “colossal” effects, very similarly in spirit as it occurs in manganites. Consider a typical clustered state (Fig. 5(b)) found by MC simulations in the disordered region. This state has preformed local SC correlations – nanoscale regions having robust SC amplitudes within each region, but no SC phase coherence between different regions – rendering the state globally non-SC (the averaged correlation at the largest distances available,  $C_{\text{SC}}^{\text{max}}$ , is nearly vanishing). Let us now introduce an artificial SC “external field”, which can be imagined as caused by the proximity of a layer with robust SC order (e.g., comprised of a higher- $T_c$  material). In practice, this is achieved in the calculations by introducing a term  $|\Delta_{\text{SC}}^{\text{ext}}|\sum_i\rho_1(\mathbf{i},\hat{z})|\Delta_i|\cos(\Psi_i)$ , where  $\Delta_{\text{SC}}^{\text{ext}}$  acts as an external field for SC. The dependence of  $C_{\text{SC}}^{\text{max}}$  with  $\Delta_{\text{SC}}^{\text{ext}}$  is simply remarkable (Fig. 5(a)). While at points  $e$  and  $f$ , located far from the SC region in Fig. 4a, the dependence is the expected one for a featureless state (linear), the behavior closer to SC and small temperatures is highly nonlinear and unexpected. For example, at point  $a$ ,  $C_{\text{SC}}^{\text{max}}$  vs.  $\Delta_{\text{SC}}^{\text{ext}}$  has a slope (at  $\Delta_{\text{SC}}^{\text{ext}}=0.02$ ) which is  $\sim 250$  times larger than at  $e$  ( $\sim 13$  times larger than at  $W=0$ , same  $T$ ,  $\rho_2$ , and  $u_{12}$ ).

The reason for this anomalous behavior is the clustered nature of the states. This is shown in the state Fig. 5(c), contrasted with (b), where a relatively small field – in the natural units of the model – nevertheless led to a quick alignment of SC phases, producing a globally SC state, as can be inferred from the uniform color of the picture. *Having preformed SC puddles vastly increases the SC susceptibility.* Since Fig. 5(a) was obtained in a trilayer geometry it is tempting to speculate that the proximity of SC layers to a non-SC but clustered state, can naturally lead to a GPE over long distances, as observed experimentally in a similar geometry.<sup>5-7</sup>

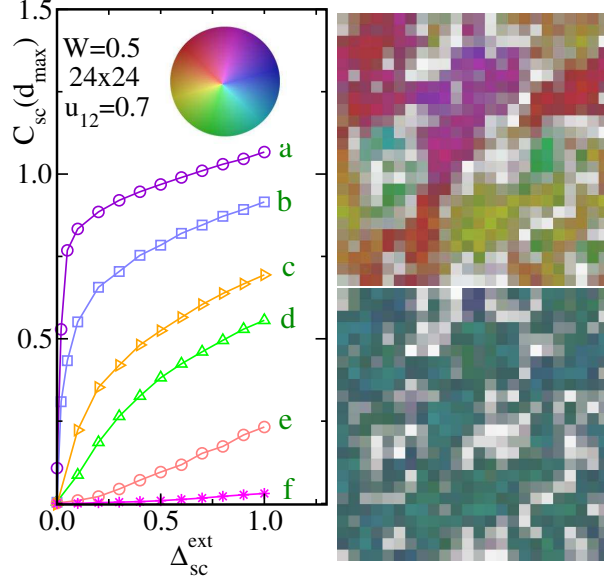


**Figure 5.** *Left:*  $C_{\text{sc}}^{\text{max}}$  vs.  $\Delta_{\text{sc}}^{\text{ext}}$  (see text) on a  $24 \times 24$  lattice, with  $u_{12}=0.7$  and  $W=0.5$ , at the five points *a-f* indicated in Fig. 4a. A “colossal” effect is observed in *a* and *b* where the  $\Delta_{\text{sc}}^{\text{ext}}=0$  state is “clustered”. A much milder (linear) effect occurs far from the SC phase (*e* and *f*). MC snapshots are shown at  $\Delta_{\text{sc}}^{\text{ext}}=0.0$  *right, top* and  $\Delta_{\text{sc}}^{\text{ext}}=0.2$  *right, bottom*, both at  $T=0.1$  and  $\rho_2=0.5$ , using the same quenched-disorder configuration. The color convention is explained in the circle (colors indicate the SC phase, while intensities are proportional to  $\text{Re}(\Delta_i)$ ). The AF order parameter is not shown. The multiple-color nature of the upper snapshot, reflects a SC phase randomly distributed (i.e. an overall non-SC state). However, a small external field rapidly aligns those phases, leading to a coherent state (*bottom*) (From Ref. 8).

## 5. DEPENDENCE OF $T_c$ WITH THE NUMBER OF LAYERS

The nanoscale clusters also leads to a proposal for explaining the *rapid* increase of  $T_c$  with the number of Cuprate layers  $N_\ell$ , found experimentally, at least up to 3 layers. In this effort, the MC phase diagrams of single-, bi-, and tri-layer systems described by Eq. (4), with and without disorder, were calculated using exactly the same parameters (besides a coupling  $\rho_2(\mathbf{i}, \hat{z})$ , equal to those along  $\hat{x}$  and  $\hat{y}$ , to connect the layers). It was clearly observed that *the single layer has a substantially lower  $T_c$  than the bilayer*. This can be understood in part from the obvious critical fluctuations that are stronger in 2D than 3D. But even more important, cluster percolation at  $W \neq 0$  is more difficult in 2D than 3D (since otherwise 2D disconnected clusters may become linked through an interpolating cluster in the adjacent layer). Then, in the phenomenological approach presented here it is natural that  $T_c$  increases fast with  $N_\ell$ , when changing from 1 to 2 layers as shown in Fig. 6a. This concept is even *quantitative* – up to a scale – considering the similar shape of  $T_c$  vs.  $N_\ell$  found both in the MC simulation and in experiments (see Figs.6b-c. Note that the subsequent decrease of  $T_c$  for 4 or more layers observed experimentally could be caused by inhomogeneous doping, beyond our model). *Our MC results suggest that the large variations of  $T_c$ 's known to occur in single-layer cuprates can be attributed to the sensitivity of 2D systems to disorder*. As  $N_\ell$  increases (the system becomes more 3D), the influence of disorder *decreases*, both in experiments<sup>34</sup> and simulations.

## 6. SPECTRAL FUNCTIONS IN THE PRESENCE OF COMPETING STATES

In this section, we will present the analysis of the one-particle spectral function,  $A(\mathbf{k}, \omega)$ , for several regimes of the phase diagram of Eq. (1). The discussion here follows closely Ref. 14. For general doping and interaction values this can only be done with the MC procedure described in Section 2.  $A(\mathbf{r}, t)$  is defined by the expression:

$$A(\mathbf{r}, t) = \langle \sum_{\mathbf{l}} c_{\mathbf{l}\sigma}^\dagger(t) c_{\mathbf{l}+\mathbf{r}, \sigma} + H.c. \rangle . \quad (5)$$

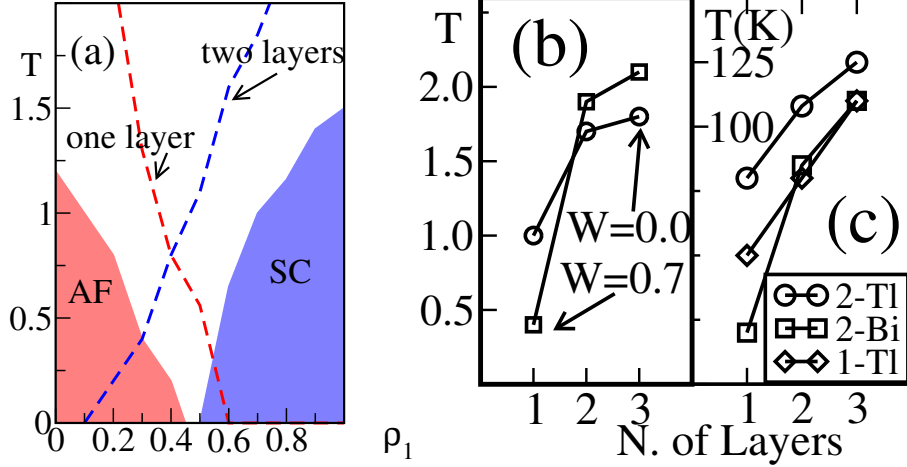


**Figure 6.** (a) MC phase diagram (for Eq.(4)) at  $u_{12}=0.7$ . Parameters are  $r_1=-1$ ,  $r_2=-0.85$ ,  $u_1=u_2=1$ ,  $W = 0.5$  with one layer (solid colors) and two layers (dashed line). The addition of an extra layer increases the critical temperature of the superconductor as well as the Néel temperature. (b)  $T_c$  vs.  $N_\ell$  for  $u_{12}=0.7$ ,  $\rho_2=0.3$ ,  $W=0.7$ , and  $24^2 \times N_\ell$  clusters. Shown are results with and without disorder. (c) The experimental  $T_c$  (in K) is shown for three HTS families, as indicated, up to 3 layers (data from Ref. 35).

Applying the modified BdG transformation, Eq. (2), Eq. (5) is calculated using:

$$A(\mathbf{r}, \omega) = \sum_n X_n(\mathbf{r})\delta(\omega - E_n^\dagger) + Y_n(\mathbf{r})\delta(\omega + E_n^\dagger), \quad (6)$$

where

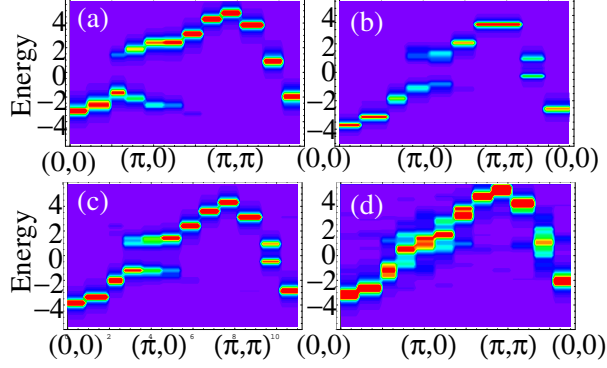
$$X_n(\mathbf{r}) = \sum_{\mathbf{l}} a_n^*(\mathbf{l})a_n(\mathbf{l} + \mathbf{r}), \quad (7)$$

and a similar expression is valid for  $Y_n$ . Eq. (6) can be Fourier-transformed to obtain  $A(\mathbf{k}, \omega)$ , but it is faster to do that after taking the average, and that route has been followed in the present work.

## 6.1. Clean System

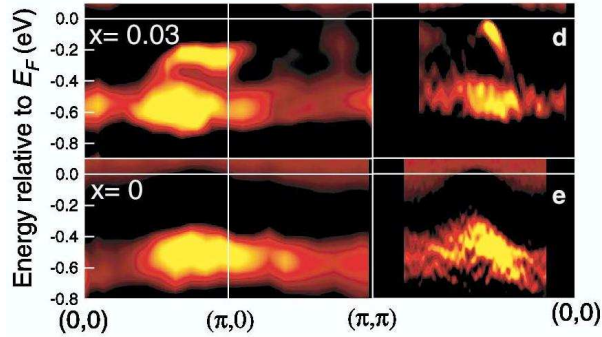
The phase diagram of Eq. (1) for the clean case (i.e. without quenched disorder) was presented in Fig. 1. The figure shows two “paths”, which describe the transition from the AF to the SC phase. The first one crosses a region of long-range order with *local* AF/SC coexistence, whereas the second one involves an intermediate “stripe” state.<sup>22</sup> We do not discuss here the exact nature of the stripe state, which may be horizontal or diagonal, depending on parameters such as doping and lattice size. For our purposes it is sufficient that an inhomogeneous state - stripe, PS or CO - exists, and what its effects are with regards to experimental probes. Four representative points along those two paths (see Fig.1) were chosen and the corresponding spectral functions calculated.

Figure 7(a) shows  $A(\mathbf{k}, \omega)$  for the purely SC case ( $J = 0$ ) for  $\mu = -1$ , leading to a uniform density  $\langle n \rangle \approx 0.7$ . Fig. 7(b) is for the case when the system presents *local* AF/SC coexistence (namely, both o.p.s simultaneously nonzero at the same site) and Fig. 7(c) for the pure AF phase. The red color indicates large spectral weight, whereas the blue one indicates very low intensity. In Fig. 7(c), the AF gap can be clearly identified, together with the typical dispersion of the AF (upper branch),  $E_{\mathbf{k}} = \pm \sqrt{\epsilon_{\mathbf{k}}^2 + J^2}$ , which makes  $E_{\mathbf{k}}$  gapped everywhere. This is in stark contrast to Fig. 7(a), where there are electronic states with appreciable intensity near the Fermi energy ( $E_F$ ) close to  $(\pi/2, \pi/2)$ , allowed by the symmetry of the pairing state. The “intermediate” state with local AF/SC coexistence is not drastically different from the one with AF correlations only, and its resulting energy dispersion can be simply described by  $E_{\mathbf{k}} = \pm \sqrt{(\epsilon_{\mathbf{k}} - \mu)^2 + J^2 + \Delta_{\mathbf{k}}^2}$  once  $\Delta_{\mathbf{k}}$  is known. This conclusion is not supposed to change using the SO(3)-symmetric spin model.



**Figure 7.**  $A(\mathbf{k}, \omega)$ , evaluated via MC, on an  $8 \times 8$  lattice for (a)  $(J, V, \mu) = (0, 1, -1)$  (SC state), (b)  $(J, V, \mu) = (0.6, 0.7, -0.4)$ , coexisting AF/SC state, (c)  $(J, V, \mu) = (0.7, 0.65, -0.3)$  (AF), and (d)  $(J, V, \mu) = (1, 0.5, -1.2)$ , striped state. (From Ref. 14)

Similarly, along path 2 of Fig. 1 a point in the phase diagram with striped order was chosen, and the corresponding spectral density is given in Fig. 7(d). This result compares very well with previous calculations, (Ref. 36, Fig. 7): for instance, the system presents a Fermi surface crossing near  $(\pi, 0)$ . Whereas the results from Fig. 7(a),(c) refer to generally well-understood phases of the cuprate phase diagram, Figs. 7(b),(d) are of relevance for the discussion related to the intermediate state, since they are both candidates for the intriguing phase in between.



**Figure 8.** Experimental ARPES spectra for LSCO with  $x = 0$  and  $x = 0.03$ . Note the development of a (flat) second high-intensity branch near  $(\pi, 0)$  and the emergence of a strongly dispersive signal at the Fermi level as the system is doped away from the half-filled insulator (reproduced from Ref. 32).

For comparison, ARPES data from Ref. 32 for  $\text{La}_{2-x}\text{Sr}_x\text{CuO}_4$  are reproduced in Fig. 8. For very low doping  $x = 0.03$  (just inside the spin-glass insulating (SGI) phase) a *flat band* is observed close to  $-0.2\text{eV}$  in addition to a *lower branch* (energy  $\sim -0.55\text{eV}$ ), which is already present in the  $x = 0$  limit and therefore can be safely identified with the lower Hubbard band. As  $x$  is increased even further, the lower branch retains its energy position, but gradually loses its intensity until it is almost completely invisible after the onset of the SC phase at  $x=0.06$ .<sup>37</sup> In contrast, the second branch gains in intensity with doping, and also moves continuously *closer* toward the Fermi level; at the same time it starts to develop a coherence peak, which is clearly visible for optimal doping. The main experimental result here, namely *the existence of two branches near  $(\pi, 0)$ , cannot be reproduced using spatially homogeneous models* as demonstrated above. The cases of AF, SC and coexisting AF+SC states all show only one branch below  $E_F$  nearby  $(\pi, 0)$ . This was already seen in Fig. 7(a)-(c) for the MC data and is seen again in the exact dispersion for those ordered phases.<sup>8</sup>

If stripe configurations are considered, as in Fig. 7(d) (MC data), there will appear two branches near  $E_F$ ,

but the form of the dispersion is clearly different from the experimental data in Fig. 8. The same occurs if instead of using data from a Monte Carlo simulation, a perfect stripe configuration is studied as in Ref.<sup>8</sup> The investigation of  $A(\mathbf{k}, \omega)$  for a spin-fermion model, related to Eq. (1), with  $\Delta_{i,\alpha} = 0$  but retaining the SO(3) spin symmetry, has been done carefully in Ref. 36. Again, stripe phases were found for certain parameters and while in some cases the existence of two branches near  $(\pi, 0)$  was reported, certainly there are no indications of “nodal” quasiparticles at  $(\pi/2, \pi/2)$ . Then, stripes alone are not an answer to interpret the results of Yoshida *et al.* As a consequence, we conclude that neither local AF+SC coexistence nor stripes can fully account for the ARPES results in the low-doping limit and alternative explanations should be considered.

Beyond the results already described, ARPES also provides surprising insights/results for momenta other than  $(\pi, 0)$  (Fig. 8). Along the Brillouin zone diagonal, a dispersive band crossing  $E_F$  is found already in the SGI phase. The FS-like feature consists of a small arc centered at  $\sim (\pi/2, \pi/2)$ ; surprisingly, as more holes are added, this arc does not expand, but simply gains spectral weight. This increase in spectral intensity is roughly proportional to the amount of hole-doping for  $x \leq 0.1$ , although it grows more strongly thereafter. This observed increase in spectral weight is in relatively good agreement with the hole concentration  $n_H$  derived from Hall measurements and was interpreted as a confirmation of the hole transport picture. Below, however, we will provide a different explanation for this behavior.

The aforementioned large gap ( $\Delta \approx 0.2\text{eV}$ ) at  $(\pi, 0)$ , together with the existence of the apparent gapless excitations around  $(\pi/2, \pi/2)$  is the essence of the PG problem. The shrinking of this gap and the concomitant appearance of a coherence peak has, for example, been interpreted as the evolution of a strongly coupled SC (at low doping) into a conventional BCS-SC at optimal doping. In this scenario, the large gap size directly reflects a large pairing scale, whereas the smallness of  $T_c$  is attributed to the preponderance of phase-fluctuations in such a regime, which would outrule the existence of a phase-coherent SC condensate at higher temperatures. Alternatively, this gap may be regarded as the signal of a hidden order, which is not otherwise manifested. In other words, the relatively large excitation gap  $\Delta_{\text{PG}}$  is explained in terms of (i) a large SC gap  $\Delta_{\text{PG}} = \Delta_{\text{SC}}$  itself, or (ii)  $\Delta_{\text{PG}} = \Delta_{\text{SC}} + \Delta_{\text{ho}}$ , with a large,  $x$ -dependent hidden order gap  $\Delta_{\text{ho}}$  whereas (iii) a mixed-state scenario, strongly influenced by disorder, leaves open the possibility that it is the (local) chemical potential that determines the PG physics. The precise role of  $\mu$  in mixed-state phases needs to be examined further, but will not be addressed here.

## 6.2. Quenched Disorder

Since calculations for  $A(\mathbf{k}, \omega)$  in the clean limit do not agree with ARPES measurements, we turn our attention to a system with quenched disorder. The impact of quenched disorder is realized by tuning the coupling constants  $J_i$  and  $V_i$  in Eq.(1), as explained in Section 2.

When disorder is added, (the reader should study again Fig. 3) a region between the SC and AF phases opens, where none of the competing order dominates and both regimes coexist in a spatially separated, mixed-phase state. This “glassy” state was discussed in detail in Section 2, where it was suggested that it leads to “colossal effects”. The pronounced susceptibility of such mixed-phase states towards applied “small” perturbations is well-known and is, e.g., often regarded as the driving force behind “colossal magneto-resistance” in manganites.<sup>10</sup>

To simplify the study and be able to access larger systems, we will consider a single SC cluster embedded in an AF background and also consider a fixed or “frozen” configuration of the classical fields (both AF and SC). Later, we will lift this restriction and perform a MC study. When a  $12 \times 12$  SC region is placed on an AF background (total lattice size is  $22 \times 22$ ), the resulting distribution of  $A(\mathbf{k}, \omega)$  is as shown in Fig. 9(a). The contribution from the AF background is clearly distinguishable from that of the SC island, since it is present even when the SC region is removed. The SC cluster induces a second “flat band” - quite typical for gapped systems - near  $E_F$ , along the  $(0, 0) \rightarrow (\pi, 0)$  direction. That this flat band is indeed produced by the SC island is verified by decreasing the size of the island to  $8 \times 8$  (Fig. 9b),  $7 \times 7$  (Fig. 9c) and finally for  $5 \times 5$  (Fig. 9d), upon which this signal gradually decreases (the cases  $9 \times 9$  and  $11 \times 11$  give very similar results to  $12 \times 12$  and are not shown.). The spectral intensity related to the surrounding AF “bath” concurrently decreases, in agreement with experimental observations.<sup>37</sup>

Therefore, even the simplest possible *mixed-phase state can qualitatively account for the observed ARPES data*. It is also interesting to note that SC signals comparably in strength with the ones stemming from the AF

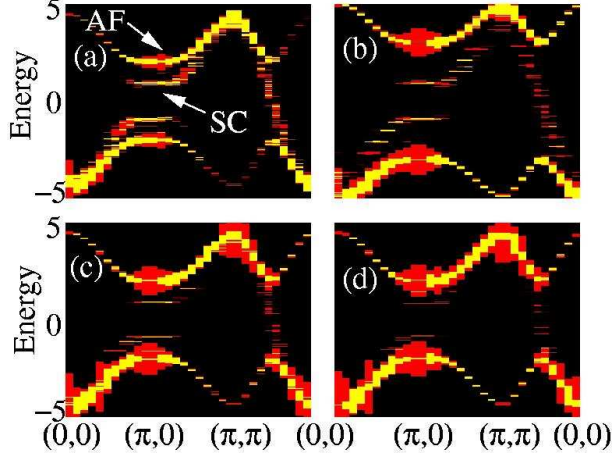


**Figure 9.** Distribution of  $A(\mathbf{k}, \omega)$  for a single configuration of classical fields, corresponding to a SC region of size (a)  $12 \times 12$ , (b)  $8 \times 8$ , (c)  $7 \times 7$  or (d)  $5 \times 5$  on a  $22 \times 22$  lattice (i.e., 30%, 15%, 10% or 5% SC respectively). Shown is  $E$  vs.  $\mathbf{k}$  along  $(0,0) \rightarrow (\pi,0) \rightarrow (\pi,\pi) \rightarrow (0,0)$ . (From Ref. 14)

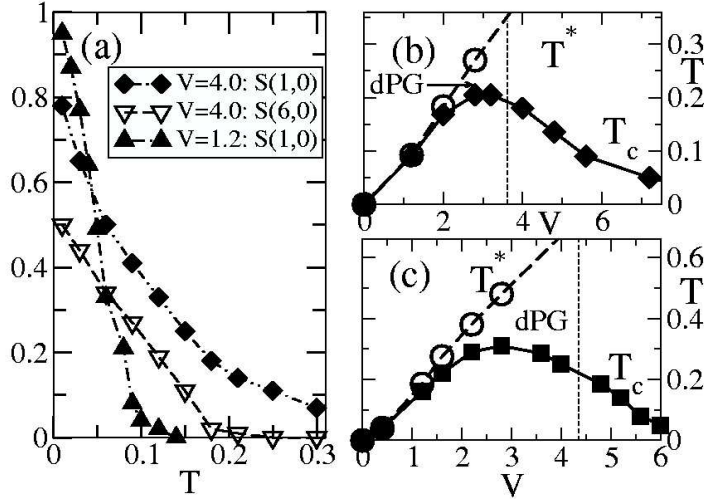


**Figure 10.** (a) Short and long range phase correlation functions,  $S(0,0)$  and  $S(6,0)$  respectively, vs.  $T$  for two different values of  $V$ , covering the weak- and strong- coupling regime, for  $\langle n \rangle = 1$ . Once  $V \leq 2$ , no difference between short- and long-range correlations is observed, and  $S(6,0)$  ( $V = 1.2$ ) is not shown for reasons of clarity. Symbol sizes roughly match the errors. (b) The phase diagram for Hamiltonian Eq. (1) with  $J = 0$  derived from (a);  $T_c$  and  $T^*$  as explained in the text. (c) shows the phase diagram for the model with a strict  $d$ -wave ground state. Note the differences between (b) and (c). The  $d$ -wave pseudo-gap regime is indicated in both (b) and (c). (Reproduced from Ref. 15)

band, are only found for rather large SC blocks, encompassing at least 20% space of the whole system. From this point of view, even in the strongly underdoped limit at  $x=0.03$ , the relative amount of the SC phase has to be quite substantial already.

## 7. STRONG COUPLING REGIME OF $D$ -WAVE SUPERCONDUCTORS

The appearance of a  $T^* > T_c$  (Fig. 3) was observed in a system with disorder and was connected with the existence of a pseudo-gap and the density-of-states as well as the formation of short range order. In this section, we revisit the study of the temperature scale  $T^*$  without quenched disorder focusing on the regime of large coupling,  $V_i = V \forall i$ . We will also consider Eq. (1) in the case  $J_i = 0$ , i.e., without magnetization terms, to

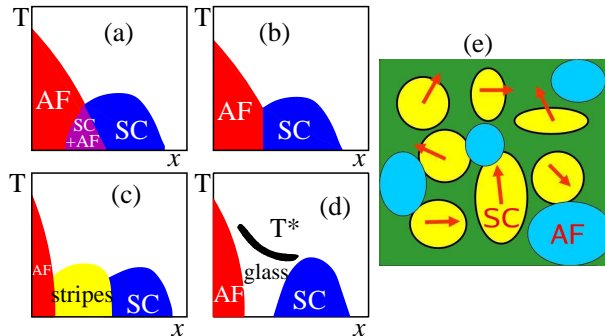


**Figure 11.** Schematic representation of the phase diagrams that our models show in the clean (a,b,c) and dirty (d) limits. The theory discussed in this paper shows the possible appearance of regions with *local* coexistence of AF and SC (panel a), or a first-order transition separating AF from SC (panel b) with the first-order character of the transition possibly continuing in the AF-disordered and SC-disordered transitions, or an intermediate striped regime (panel c). Possibilities (a) and (b) have already been discussed in Ref. 21, although here we do not invoke a higher symmetry group such as SO(5). The main result contain in this figure is the proposed phase diagram in the presence of quenched disorder (panel d). Shown are the glassy region, proposed to be a mixture of SC and AF clusters, and the  $T^*$  where local order starts upon cooling. This phase diagram has similarities with those proposed before for manganites,<sup>9,10</sup> and certainly it is in excellent agreement with the experimental phase diagram of LSCO. (b) Schematic representation of the “glassy” state that separates the SC and AF regions. The arrow indicates the phase of the SC order parameter.

compare this results with the usual BCS regime. It is important to remark again that the approach is built<sup>15</sup> on the insight that this Hamiltonian is quadratic in fermionic operators and thus can be efficiently studied with the help of Monte Carlo techniques explained before. This is possible here because the original interacting model has been stripped down of quantum fluctuations in the pairing approximation. But after that approximation is made the treatment is exact within numerical errors.

The investigation of the temperature dependence of  $C(m)$ , Eq. (3) for Hamiltonian Eq. (1), allows for the introduction in a BCS-like Hamiltonian two characteristic temperatures  $T^*$  and  $T_C$  in the case of strong coupling, in contrast to the BCS regime, where the distinction does not exist. We associate  $T^*$  with the temperature where short-range phase correlations develop (defined here as  $C(|m|=1) \geq 0.1$ , but other cutoffs leads to quite similar qualitative conclusions). On the other hand,  $T_C$  is commonly identified with the onset of long-range (LR) phase coherence (here we use the criterion  $C(|m|=max) \geq 0.1$ .  $T^*$  and  $T_C$  are essentially identical for  $V$  not too large, Fig. 10a, and they are only clearly different for  $V \gtrsim 3$ , with  $T^*$  larger than  $T_C$  by a factor of 3-4 for  $V > 5$ . This works in the low- $\langle n \rangle$  limit, too. Based on MC results, a phase diagram, presenting  $T^*$  and  $T_C$  as a function of the pairing attraction, is displayed in Fig. 10b-c. Remarkably, the values of  $T_C$  reach a maximum  $T_C^{max} \simeq 0.2$  for  $V_{max} \approx 3$ , whereas  $T^*$  increases steadily with increasing  $V$ . We have also considered a model where  $\Delta_{i,x} = -\Delta_{i,y}$ , *i.e.*, enforcing a  $d$ -wave ground state. For this restricted model, Fig. 10c,  $T_C^{max} \simeq 0.3$ , with a more prominent regime of short range correlations.

Although the existence of  $T_C^{max}$  has long been known, it has been directly established for the first time very recently in Ref. 15, since traditional self-consistent methods are tracking  $T^*$  rather than  $T_C$ . Yet, as demonstrated in Fig. 10, those mean field methods work very well for  $V$  not very strong.

For  $V \gtrsim V_{max}$  the system presumably enters the realm of pronounced Kosterlitz-Thouless physics,<sup>38</sup> whence  $T_C$  is dictated by vortex binding rather than Cooper pairing. The critical temperature  $T_{KT} = T_C$  in such models is proportional to  $1/V$ , following a perturbative analysis, similar to what is found in Fig. 10b-c. In this context, it is unclear whether or not KT behavior is found for Eq. (1) (with  $J_i = 0$ ) which unlike in the standard XY model, couples fermions to classical fields. However, there is indication from the numerical analysis<sup>15</sup> that KT physics is indeed relevant in the region between  $T_C$  and  $T^*$ .

## 8. CONCLUSIONS

Summarizing, here simple phenomenological models for phase competition showed that – depending on details – different cuprates could have stripes, local coexistence, first-order transitions, or a glassy clustered state interpolating between AF and SC phases. Figure 11a illustrates our proposed possibilities. In Cu-oxides where the glass state is realized, namely where we believe SC puddles could be present, this study revealed the possibility of colossal effects. A schematic representation of the proposed glassy state with colossal effects is in Fig. 11b. This proposal could provide rationalization of recent results in trilayer thin-film geometries.<sup>5–7</sup>

Other interesting experimental and theoretical efforts that complement the discussion presented here are: *(i)* In Ref. 39, further evidence of an anomalous proximity effect in the cuprates is presented. These results add to those of Ref. 5–7, showing that the anomalous effects are real. *(ii)* In Ref. 40, 41, the phase diagram of YBCO was recently investigated in the presence of Ca doping. Among many results, it was shown that a glassy state is generated between the AF and SC states in Ca-doped YBCO, with a phase diagram very similar to that in LSCO and our Fig. 11(d). This result suggests that *Ca-undoped* YBCO may have either a region of local coexistence of SC and AF or a first-order transition separating them (as in Fig. 11(a,b)), and only with the help of extra quenched disorder is that a glassy state is generated. Then, the generic phase diagram of the cuprates – which usually is considered to be that of LSCO – may not be as universal as previously believed, as discussed in this publication. Our study showing that bilayered systems are more stable than single layers with respect to disorder is also compatible with the experimental results of Ref. 40, 41, namely the 1-layer material is more likely to have a glassy state between AF and SC than 2- or higher layer materials. *(iii)* Electronic inhomogeneity and competing phases in electron-doped superconducting have been reported<sup>42</sup> for  $\text{Pr}_{0.88}\text{LaCe}_{0.12}\text{CuO}_4$ . *(iv)* Our effort has already induced interesting theoretical work<sup>43</sup> in the context of  $J$ - $U$  models. *(v)* Theoretical work<sup>44</sup> closely related to our proposed glassy state in Fig. 11 has addressed inhomogeneous Josephson phases near the superconductor-insulator transition. *(vi)* Recent neutron and Raman scattering investigations applied to  $\text{La}_2\text{CuO}_{4.05}$  has shown the coexistence of SC and AF phases in this compound.<sup>45</sup> *(vii)* Finally, our results have similarities with those recently discussed in the context of *Bose metals* as well.<sup>46</sup>

The study also provided implications of these numerical calculations for photoemission experiments and a simple explanation for the  $T_c$  increase with  $N_\ell$  (another explanation can be found in Ref. 47).

A Monte Carlo technique<sup>15</sup> was reviewed for an unbiased investigation of the SC state as described in the pairing Hamiltonian. It reproduces the BCS limit as well as the strong-coupling regime at all temperature and densities. The establishment of a pseudo-gap regime in the case of a strong pairing between two characteristic temperatures  $T^*$  and  $T_C$  and an associated nontrivial phase diagram has been numerically demonstrated. These results seem to indicate that the observed pseudo-gap features of HTSs cannot be reconciled with a classical phase-fluctuation-dominated  $d$ -wave superconductivity.

Clustered states are crucial in manganites and other compounds,<sup>48</sup> and this analysis predicts its potential relevance in HTS materials as well. The theoretical and experimental investigations of transition metal oxides in recent years are unveiling self-organized phenomena that usually manifest in the form of inhomogeneous states, revealing the intrinsic complexity of cuprates and manganites, and likely several other transition metal oxides.

## ACKNOWLEDGMENTS

The Oak Ridge National Laboratory is managed by UT-Battelle, LLC, for the U.S. Department of Energy under Contract DE-AC05-00OR22725. A. M. and E. D. are supported by NFS grant DMR-0312333.

## REFERENCES

1. J. M. Tranquada, B. J. Sternlieb, J. D. Axe, Y. Nakamura, and S. Uchida, “Evidence for stripe correlations of spins and holes in copper oxide superconductors,” *Nature* **375**, p. 561, 1995.
2. V. Emery, S. A. Kivelson, and H. Q. Lin, “Phase separation in the t-j model,” *Phys. Rev. Lett.* **64**, p. 475, 1990.
3. K. Lang, V. Madhavan, J. E. Hoffman, E. W. Hudson, H. Eisaki, S. Uchida, and J. C. Davis, “Imaging the granular structure of high-Tc superconductivity in underdoped  $\text{Bi}_2\text{Sr}_2\text{CaCu}_2\text{O}_{8+\delta}$ ,” *Nature* **415**, p. 412, 2002.

4. Y. Kohsaka, K. Iwaya, S. Satow, T. Hanaguri, M. Azuma, M. Takano, and H. Takagi, "Imaging nano-scale electronic inhomogeneity in lightly doped mott insulator  $\text{Ca}_{2-x}\text{Na}_x\text{CuO}_2\text{Cl}_2$ ," *Phys. Rev. Lett.* **93**, p. 097004, 2004.
5. I. Bozovic, G. Logvenov, M. A. J. Verhoeven, P. Caputo, E. Goldobin, and M. Beasley, "Giant Proximity Effect in Cuprate Superconductors," *Phys. Rev. Lett.* **93**, p. 157002, 2004.
6. R. S. Decca, H. D. Drew, E. Osquiguil, B. Maiorov, and J. Guimpel, "Anomalous proximity effect in underdoped  $\text{YBa}_2\text{Cu}_3\text{O}_{6+x}$  josephson junctions," *Phys. Rev. Lett.* **85**, p. 3708, 2000.
7. J. Quintanilla, K. Capelle, and L. Oliveira *Phys. Rev. Lett.* **90**, p. 089703, 2003.
8. G. Alvarez, M. Mayr, A. Moreo, and E. Dagotto, "Areas of superconductivity and giant proximity effects in underdoped cuprates," *Phys. Rev. B* **71**, p. 014514, 2005.
9. E. Dagotto, ed., *Nanoscale Phase Separation and Colossal Magnetoresistance*, Springer Verlag, Berlin, 2002.
10. E. Dagotto, T. Hotta, and A. Moreo, "Colossal magnetoresistant materials: the key role of phase separation," *Physics Reports* **344**, p. 1, 2001.
11. Y. Tokura and N. Nagaosa *Science* **288**, p. 462, 2000.
12. G. Su and M. Suzuki *Phys. Rev. B* **58**, p. 117, 1998.
13. C. Noce and M. Cuoco *Phys. Rev. B* **59**, p. 7409, 1999.
14. M. Mayr, G. Alvarez, A. Moreo, and E. Dagotto cond-mat/0503727, 2005.
15. M. Mayr, G. Alvarez, C. Sen, and E. Dagotto, "Phase fluctuations in strongly coupled d-wave superconductors," *Phys. Rev. Lett.* **94**, p. 217001, 2005.
16. S. Sorella, G. B. Martins, F. Becca, C. Gazza, L. Capriotti, A. Parola, and E. Dagotto, "Superconductivity in the two-dimensional t-J model," *Phys. Rev. Lett.* **88**, p. 117002, 2002.
17. S. White and D. J. Scalapino, "Density matrix renormalization group study of the striped phase in the 2d t-j model," *Phys. Rev. Lett.* **80**, p. 1272, 1998.
18. W. A. Atkinson, P. J. Hirschfeld, and L. Zhu, "Quantum interference in nested d-wave superconductors: A real-space perspective," *Phys. Rev. B* **68**, p. 054501, 2003.
19. A. Ghosal, C. Kallin, and A. J. Berlinsky, "Competition of superconductivity and antiferromagnetism in a d-wave vortex lattice," *Phys. Rev. B* **66**, p. 214502, 2002.
20. M. Ichioka and K. Machida, "Electronic structure of stripes in two-dimensional hubbard model," *J. Phys. Soc. Jpn.* **68**, p. 4020, 1999.
21. S. Zhang, "A unified theory based on  $SO(5)$  symmetry of superconductivity and antiferromagnetism," *Science* **275**, p. 1089, 1997.
22. M. Moraghebi, S. Yunoki, and A. Moreo, "Robust d-wave pairing correlations in a hole-doped spin-fermion model," *Phys. Rev. Lett.* **88**, p. 187001, 2002.
23. J. M. T. and. D. Axel, N. Ichikawa, A. R. Moodenbaugh, Y. Nakamura, and S. Uchida, "Coexistence of, and competition between, superconductivity and charge-stripe order in  $\text{La}_{1.6-x}\text{Nd}_{0.4}\text{Sr}_x\text{CuO}_4$ ," *Phys. Rev. Lett.* **78**, p. 338, 1997.
24. D. Poilblanc and T. M. Rice *Phys. Rev. B* **39**, p. 9749, 1989.
25. J. Zaanen and O. Gunnarsson *Phys. Rev. B* **40**, p. 7391, 1989.
26. V. Emery and S. Kivelson *Physica* **209**, p. 597, 1993.
27. V. Emery and S. Kivelson *Physica* **235**, p. 189, 1994.
28. H.-D. Chen, S. Capponi, F. Alet, and S.-C. Zhang Global Phase Diagram of the High Tc Cuprates, cond-mat/0312660, 2003.
29. X. Zhou, T. Yoshida, S. A. Kellar, P. V. Bogdanov, E. D. Lu, A. Lanzara, M. Nakamura, T. Noda, T. Kakeshita, H. Eisaki, S. Uchida, A. Fujimori, Z. Hussain, and Z.-X. Shen, "Dual nature of the electronic structure of  $(\text{La}_{2-x-y}\text{Nd}_y\text{Sr}_x)\text{CuO}_4$  and  $\text{La}_{1.85}\text{Sr}_{0.15}\text{CuO}_4$ ," *Phys. Rev. Lett.* **86**, p. 5578, 2001.
30. E. Demler, S. Sachdev, and Y. Zhang, "Spin-ordering quantum transitions of superconductors in a magnetic field," *Phys. Rev. Lett.* **87**, p. 067202, 2001.
31. Y. Sidis, C. Ulrich, P. Bourges, C. Bernhard, C. Niedermayer, L. P. Regnault, N. H. Andersen, and B. Keimer, "Antiferromagnetic ordering in superconducting  $\text{YBa}_2\text{Cu}_3\text{O}_{6.5}$ ," *Phys. Rev. Lett.* **86**, p. 4100, 2001.

32. T. Yoshida, X. J. Zhou, T. Sasagawa, W. L. Yang, P. V. Bogdanov, A. Lanzara, Z. Hussain, T. Mizokawa, A. Fujimori, H. Eisaki, Z.-X. Shen, T. Kakeshita, and S. Uchida, "Metallic behavior of lightly doped  $\text{La}_{2-x}\text{Sr}_x\text{CuO}_4$  with a Fermi surface forming an arc," *Phys. Rev. Lett.* **91**, p. 027001, 2003.
33. A. Hossein, D. Broun, D. Sheehy, T. Davis, M. Franz, R. Liang, W. Hardy, and D. Bonn cond-mat/0312542, 2003.
34. H. Eisaki, N. Kaneko, D. Feng, A. Damascelli, P. Mang, K. Shen, Z.-X. Shen, and M. Greven cond-mat/0312570, 2003.
35. G. Burns, *High-Temperature Superconductivity: An Introduction*, Academic Press, Inc., San Diego, CA, 1992.
36. M. Moraghebi, S. Yunoki, and A. Moreo, "Fermi surface and spectral functions of a hole-doped spin-fermion model for cuprates," *Phys. Rev. B* **63**, p. 214513, 2001.
37. A. Ino, C. Kim, M. Nakamura, T. Yoshida, T. Mizokawa, Z.-X. Shen, A. Fujimori, T. Kakeshita, H. Eisaki, and S. Uchida, "Electronic structure of  $\text{La}_{2-x}\text{Sr}_x\text{Cu}_4$  in the vicinity of the superconductor-insulator transition," *Phys. Rev. B* **62**, p. 4137, 2000.
38. J. Kosterlitz and D. Thouless *J. Phys. C* **6**, p. 1181, 1973.
39. I. Asulin, A. Sharoni, O. Yulli, G. Koren, and O. Millo *Phys. Rev. Lett.* **93**, p. 157001, 2004.
40. S. Sanna, G. Allodi, G. Concas, and R. D. Renzi The Underdoped Region of the Phase Diagram of  $\text{YBa}_2\text{Cu}_3\text{O}_{6+x}$ , 2004.
41. S. Sanna, G. Allodi, G. Concas, A. Hillier, and R. D. Renzi cond-mat/0403608, 2004.
42. P. Dai, H. J. Kang, H. A. Mook, M. Matsuura, J. W. Lynn, Y. Kurita, S. Komiya, and Y. Ando *Phys. Rev. B* **71**, p. 100502(R), 2005.
43. L. Arrachea and D. Zanchi cond-mat/0409141, 2004.
44. J. Tu, M. Strongin, and Y. Imry An Inhomogeneous Josephson Phase near the (Super)Conductor-Insulator Transition, preprint, 2004.
45. V. Gnezdilov, Y. Pashkevich, J. Tranquada, P. Lemmens, G. Güntherodt, A. Yeremenko, S. Barilo, S. Shiryayev, L. Kurnevich, and P. Gehring cond-mat/0403340, 2004.
46. P. Phillips and D. Dalidovich *Science* **302**, pp. 243–247, 2003.
47. S. Chakravarty, H.-Y. Kee, and K. Völker *Nature* **428**, p. 53, 2004.
48. H. Rho, C. S. Snow, S. L. Cooper, Z. Fisk, A. Comment, and J.-P. Ansermet *Phys. Rev. Lett.* **88**, p. 127401, 2002.